History-dependent volcanic ground deformation from broad-spectrum viscoelastic rheology around magma reservoirs

Yang Liao[1], Leif Karlstrom[2], Brittany A. Erickson[2,3]

[1]Department of Geology and Geophysics, Woods Hole Oceanographic Institution
[2]Department of Earth Sciences, University of Oregon
[3]Department of Computer Science, University of Oregon

Key Points:

- New analytic framework for deformation from pressure forcing of a magma chamber in a viscoelastic crust with temperature dependent viscosity
- Analytic transfer function between reservoir pressure and surface deformation depends on frequency, viscoelastic model, and thermal profile
- Application of the transfer function reveals history dependence of deformation and elastic/viscous transition surrounding magma reservoirs

Corresponding author: Yang Liao, `yliao@whoi.edu`

Abstract

Long-duration, continuous geodetic timeseries suggest that volcanoes exhibit a wide range of deformation patterns that vary between episodes of unrest. Viscoelastic deformation around crustal magma storage zones is an expected contributor to such observations, but is challenging to characterize robustly. Here we present an analytic approach for modeling crustal deformation around magma reservoirs that highlights frequency-domain signatures of viscoelastic response for temperature-dependent crustal rheology. We develop a transfer function that links frequency spectra of chamber pressure to surface displacement, finding that properties of the magmatic system are encoded at periods where geodetic observations are routinely made. Inhomogeneous viscoelastic response is characterized by a frequency-dependent elastic-viscous transition around the reservoir. We explore the consequences of this frequency dependence by examining broadband forcing consisting of multiple impulsive pressurization episodes, and identify a history dependence of volcano deformation in which past activity influences the stress state and surface deformation of future episodes.

Plain Language Summary

Prior to eruption, magma is stored in crustal reservoirs. The mechanical evolution of such magmatic reservoirs can sometimes be inferred from timeseries of surface deformation by invoking deformation models. But such models often exhibit significant non-uniqueness, particularly over long timescales or with respect to spatially variable crustal rock properties. Here we develop a method which considers volcano deformation problem in the frequency rather than time domain. We focus on viscoelastic deformation and demonstrate that surface deformation patterns depend on the frequency of forcing as well as the prior history of deformation in the reservoir. This approach implies that aspects of the mechanical and thermal state of the crust around magma chambers may be encoded in characteristic frequency spectra of surface deformation.

1 Motivation and background

Modeling ground deformation timeseries at active volcanoes is one of the most often used approaches for inferring magma reservoir dynamics (e.g., Fernández et al., 2017; Townsend, 2022), magma properties (Hou Yip et al., 2022), and forecasting eruptions (Kilburn, 2018). While some active volcanoes exhibit deformation patterns that are well-approximated with the simplest of mechanical models for a pressurized magma chamber at depth in an elastic half-space (e.g., Mogi, 1958), additional factors are necessary to explain the spectrum of volcano deformation observed (Biggs & Pritchard, 2017). Crustal mechanical heterogeneity, surface topography and subsurface layering, and multiphase, multicomponent rheology of magma and fluids have been proposed, painting an increasingly complex picture of the shallow crustal magma transport system.

Unfortunately, many of these factors trade off when it comes to their surface expression, particularly because the deep magma flux entering reservoirs is typically unknown. Time-dependent deformation signals are challenging to interpret uniquely as due to rock creep or magma/fluid mass movements. It is a outstanding challenge in volcano geodesy therefore to characterize deformation timeseries in a self-consistent physical framework.

One general approach proposes a frequency dependent rheology of Earth materials (O'connell & Budiansky, 1978; H. C. P. Lau et al., 2020) to account for the characteristic spectrum of viscolelastic response between post-seismic and isostatic adjustment timescales (Pollitz et al., 2000; Lambeck et al., 2017), as the mechanisms and scales of deformation vary. Here we examine some implications of such a spectral domain perspective on magmatic systems. Under an appropriate description of magma chamber deformation, for example, the factors mentioned above might be viewed as linear or nonlinear spectral 'filters', which modify an input signal (e.g., a pressurization time sequence) to generate frequency and wavenumber spectra of output signals (e.g., crustal stresses, surface displacement, etc).

We derive an analytic transfer function between magma chamber pressure and maximum surface deformation, confirming the findings of Rucker et al. (2022) that frequency-dependent phase and amplitude are signatures of the viscoelastic filter. These metrics of the transfer function are shown to be sensitive to magma chamber geometry, host rock rheology, and crustal temperature field. This approach establishes a surprisingly simple link between analytic (e.g., Dragoni & Magnanensi, 1989; Segall, 2016) and numerical approaches (e.g., Del Negro et al., 2009; Gregg et al., 2013; Head et al., 2021) to viscoelastic magma chamber models.

We then demonstrate through two volcanologically-motivated examples that viscoelastic host rock response to broad-band magma chamber pressurization leads to history-dependence of surface deformation. This has implications for the interpretation of long volcano deformation timeseries, inference of crustal stress state, and eruption forecasting. We show that the elastic-ductile transition around magma chambers associated with temperature dependence of crust rheology arises via frequency-dependent partitioning of viscous and elastic crustal strains. This implies a spectral framework for investigating trans-crustal magmatic systems via ground deformation that leverages broad spectrum rheological considerations.

2 Frequency domain viscoelastic model for magma reservoir deformation

We consider a spherical magma chamber with radius r_o and depth d in a viscoelastic half space (Figure 1A). The magma chamber has a uniform interior temperature T_{in}. Steady state crustal temperature $T(r)$ is assumed radially symmetric (Figure 1A), determined by two boundary conditions $T(r_o) = T_{in}$ and $T(d) = 0$. This temperature field approximates a crustal geotherm dominated by the thermal perturbation of a magma reservoir, and becomes inaccurate at distances where the radial gradient dT/dr approaches the background vertical gradient. For a magma chamber with interior temperature of $1000-1200$°C at depth of $5-10$km and vertical geothermal gradient of $20-30$°C/km, a radially symmetric temperature profile approximates an extended region above the chamber adequately to a radius equal to the depth for some cases (see Figure S1).

Rheology of the crust is assumed Maxwell viscoelastic, with temperature-dependent viscosity that increases exponentially away from the chamber (Figure 1A and Supplement) (Del Negro et al., 2009; Karlstrom et al., 2010; Degruyter & Huber, 2014). This rheological model has been used extensively in volcano and tectonic geodesy for understanding viscoelastic response (e.g., Tromp & Mitrovica, 1999; Segall, 2010). However it is not unique and likely oversimplifies the parameterization of microscale creep mechanisms that set the relative proportions of recoverable versus non-recoverable strains for given forcing (H. C. Lau & Holtzman, 2019). We use the Maxwell model for demonstrating a theoretical framework that is transparent and simply extended to more complex rheological models.

Mechanical response, such as surface ground deformation, to forcing associated with chamber pressurization is governed by the rheology of the magma reservoir plus crust system. Time-dependent pressure forcing is a boundary condition for radial stress at r_o, which, together with an implicit boundary condition of vanishing displacement at $r = \infty$, predict a unique displacement pattern. An approximate solution for surface displacement is found via first-order correction on the full-space solution to account for stress-free surface conditions (Mogi, 1958; Del Negro et al., 2009). This is accurate so long as chamber radius to depth ratio R/D is sufficiently small (Segall, 2010).

As a starting point for modeling active systems, it is often assumed that the geometry of magma reservoirs is fixed in time and that magmatic forcing arises from magma pressurization relative to lithostatic stress. With these assumptions, viscoelastic deformation around a magma reservoir is a Linear Time-Invariant system (Schetzen, 2003) and can be solved via transfer function in the frequency domain between the unknown forcing function as input sig-

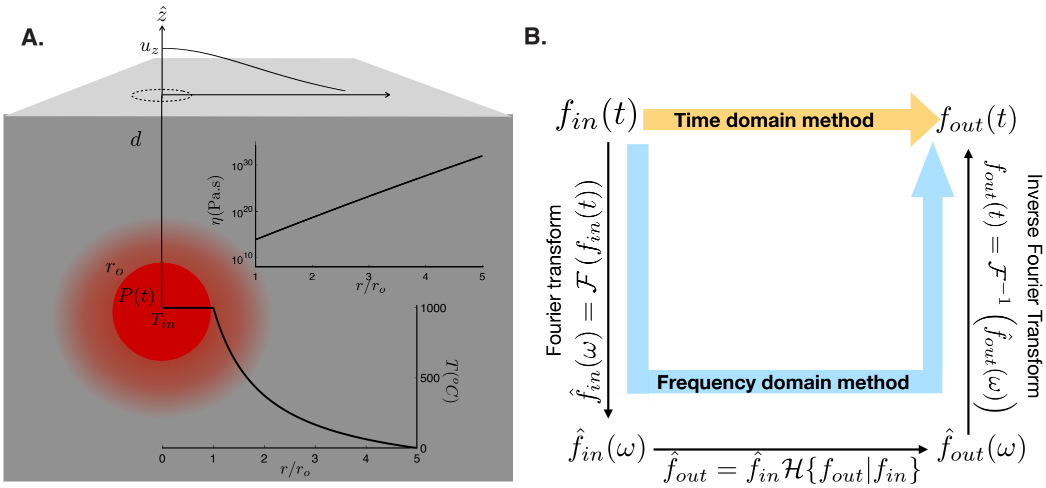

Figure 1. **A.**Geometry of the model, representative temperature, vertical surface deformation and viscosity profiles. **B.** Representation of the spectral method and transfer function approach for connecting general input and output signals f_{in} and f_{out}. The input signal is represented either in time domain (t) or frequency domain (ω), hats represent Fourier transform $\mathcal{F}$. Multiplication by transfer function $\mathcal{H}(f_{out}|f_{in})$ is the frequency domain equivalent of time domain solution to the linear governing equations.

nal and any resultant scalar mechanical output such as vertical or horizontal displacement at a point on the Earth's surface. Although in general this transfer function can be found numerically (Rucker et al., 2022), we develop an analytic transfer function for the model problem above (derived in the Supplement) to demonstrate key phenomenological outcomes of broad-spectrum viscoelastic deformation.

The transfer function $\mathcal{H}\{f_{out}(t)|f_{in}(t)\} = \hat{f}_{out}/\hat{f}_{in}$ linearly relates the frequency spectrum of an unknown quantity $\hat{f}_{out}$ (i.e., an output signal, where hat signifies Fourier transform) from the frequency spectrum of an input signal $\hat{f}_{in}$. This frequency domain method provides an equivalent approach to time-domain methods for forward and inverse problems (Figure1B). While any input or output signals can be used to compute $\mathcal{H}$, we will assume for illustrative purposes that the chamber overpressure $P(t)$ relative to lithostatic is a known input signal, and the maximum surface displacement $u_z(t)$ is the output signal (Figure 1A).

For a spherical magma chamber in an elastic halfspace, the transfer function assuming first-order free surface corrections (McTigue, 1987) may be stated as

$$\hat{u}_z^{el}(\omega) = \mathcal{H}\{u_z^{el}(t)|P(t)\}\hat{P}(\omega) = \frac{r_o^3}{\mu d^2}\frac{3K+4\mu}{6K+2\mu}\hat{P}(\omega) \tag{1}$$

where superscript el refers to linear elastic rheology, μ is shear modulus and K is the bulk modulus. The elastic transfer function is hence real-valued and independent of frequency. We are interested in isolating viscoelastic effects, and henceforth normalize transfer functions by equation 1.

Applying the constitutive relations, boundary conditions, and Fourier transform (supplement), we obtain the normalized viscoelastic transfer function $\bar{\mathcal{H}}$ between chamber pressure and maximum surface displacement

$$\bar{\mathcal{H}} = \frac{\mathcal{H}\{u_z|P\}}{\mathcal{H}\{u_z^{el}|P\}} = \left(1 - 3r_o^3 \int_{r_o}^{\infty} \frac{dr}{r^4\,(iDe(r)/\zeta + 1)}\right)^{-1}, \quad \zeta = \frac{K}{K + \frac{4}{3}\mu}. \tag{2}$$

This equation introduces the Deborah number $De(r) = \omega\eta(r)/\mu$, a dimensionless product of characteristic cyclic strain rate ($\omega > 0$) or inverse period ($\tau = 2\pi/\omega$) associated with reservoir pressurization, and Maxwell time $\eta(r)/\mu$ that measures the relative importance of viscous versus elastic response in the system. De varies with space when material properties η and/or μ vary with space, here due to the Arrhenius relationship between viscosity and temperature (Figure 1A). In general the elastic moduli K and μ also vary with temperature, but for temperature difference between 0 and $800°C$ K varies by 1% and μ varies by 10% (Bakker et al., 2016). This is small in comparison to the orders of magnitude of variation in viscosity, so we assume uniform elastic bulk moduli K and μ to keep the model simple.

From equation (2) we see that the normalized transfer function $\bar{\mathcal{H}}$ is a viscoelastic correction on the elastic displacement. The magnitude of this correction is determined by the spatial structure of Deborah number. If the crust is elastic, the viscosity is infinitely large and $De(r) = 0$ for all frequencies; in this case the normalized transfer function becomes unity.

Because crustal magmatic systems are characterized by spatially localized temperature anomalies, the transfer function defines a localized region of viscous response and implies that a near-chamber elastic/viscous transition controls viscoelastic deformation. This is the motivation behind magma chamber models that assume a discrete viscoelastic shell of uniform viscosity (Dragoni & Magnanensi, 1989; Karlstrom et al., 2010; Degruyter & Huber, 2014), a simplification of continuous variation in material properties expected in spatially variable thermal field.

We find that the general response of a material with variable viscoelastic moduli can be precisely represented by that of a discrete and uniform viscoelastic shell with frequency dependent effective viscosity and temperature under monochromatic forcing at period τ. For such case, the outer radius of the viscoelastic shell R_{eff} defining a transition to elastic response, the uniform effective temperature T_{eff} and the resulting (constant) Deborah number De_{eff} associated with viscosity $\eta_{eff}(T_eff)$ are found by requiring that the transfer function $\mathcal{H}^{eff} = (iDe_{eff} + \zeta)/(iDe_{eff} + \frac{r_o^3}{R_{eff}^3}\zeta)$ matches equation (2). Generic unsteady pressure forcing can be decomposed into superpositions of such harmonic forcing functions (Rucker et al., 2022). This result thus provides a bridge between classical analytic models and numerical approaches for magma chamber deformation.

3 Properties of the transfer function

Polar decomposition of the complex-valued $\bar{\mathcal{H}}$ calculated by (2) via $\bar{\mathcal{H}} = \mathcal{A}e^{i\varphi}$ allows for the identification of an amplification factor $\mathcal{A} = |\mathcal{H}|$ and a phase delay of $-\varphi$. These quantities completely characterize the transfer function, and provide insight into the frequency dependence of viscoelastic deformation.

Both the amplification factor and the phase delay frequency spectra vary with the physical properties of the system. Figure 2A-B shows dependence on the two parameters controlling steady-state temperature of the crust, the chamber temperature and assumed background thermal gradient (defined using a radius contour associated with chamber depth below surface). As shown in Figure 2B, $\mathcal{A}$ increases with forcing period due to increasing spatial extent of viscous response. In contrast, the frequency dependence of the phase lag is non-monotonic (Figure 2A), and peaks at a value well below the viscous fluid phase lag of $\pi/2$ (Figure 2D). Time-domain delay between deformation and harmonic pressure forcing increases monotonically with period (Supplementary figure S5).

For short forcing periods, the crust becomes more elastic hence the phase lag decreases with forcing period. As forcing period $\tau = 2\pi/\omega$ increases, the phase lag reaches a max-

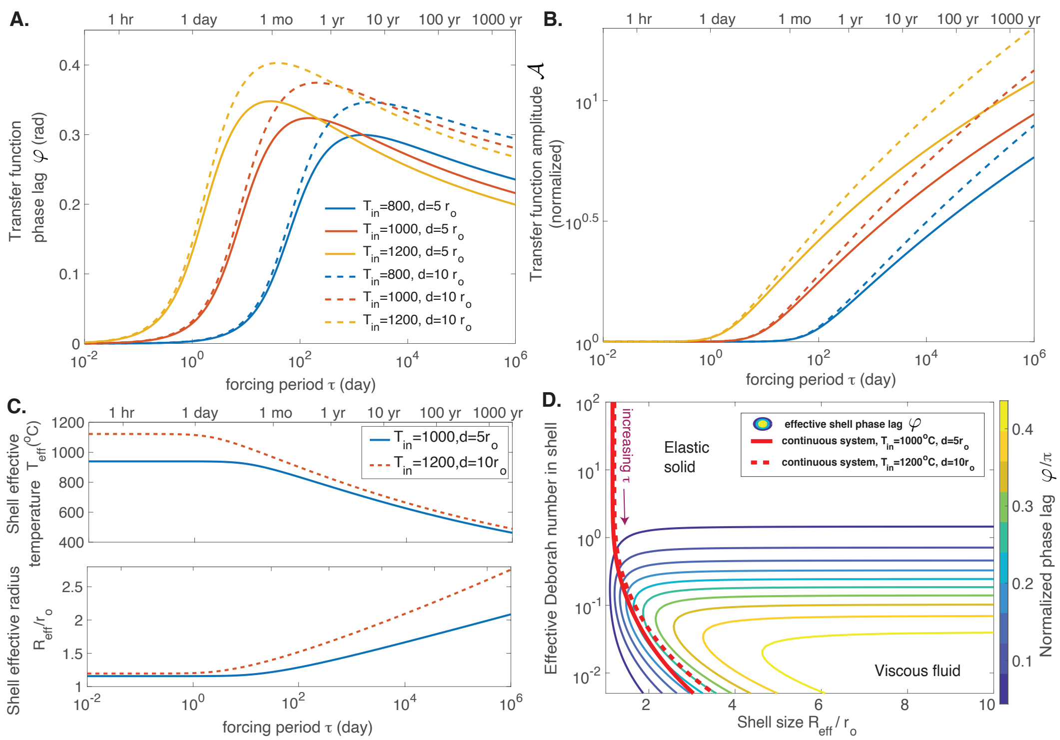

Figure 2. **A.** Phase lag φ and **B.** amplification factor $\mathcal{A}$ of the normalized transfer function $\bar{\mathcal{H}}$ calculated according to equation (2) as functions of harmonic pressure forcing period ($\tau = 2\pi/\omega$), for different chamber temperatures and depths approximated from a thermal model. **C.** Effective outer radius R_{eff} and temperature T_{eff} of equivalent discrete viscoelastic shell for harmonic pressure forcing. **D.** Phase lag φ of the transfer function as function of effective discrete viscoelastic shell radius and Deborah number in the shell (De_{eff}, colored contours). The red curves are trajectories from variable coefficient models shown in (C), illustrating that the radial viscosity profiles result sample a range of phase lags with finite maximum. The viscous fluid limit ($\varphi = \pi/2$) is not reached because viscoelastic relaxation saturates in the variable coefficient system, with effective elastic response observed at small τ and approached as $\tau \to \infty$.

imum and drops to zero as $\tau \rightarrow \infty$. This behavior can be explained by a competition between spatially confined viscous relaxation and cyclic pressure forcing. The spatial extent of viscous response R_{eff} is confined near the reservoir by the viscosity profile (set by temperature). As forcing period increases, effective temperature of the shell decreases while R_{eff} increases (Figure 2C). The timescale for viscoelastic stress relaxation over the shell $\eta_{eff}/\mu(R_{eff}/r_0)^3$ (Dragoni & Magnanensi, 1989) thus increases with forcing period, although shell effective Deborah number is dominated by τ and decreases monotonically. The increase of $\mathcal{A}$ with τ reflects viscous strain across the growing shell, with maximum viscoelastic response implicated by a maximum phase lag φ. For fixed R_{eff}, maximum phase lag occurs where $De_{eff} = \zeta(R_{eff}/r_0)^{-3/2}$ (supplement). Large forcing period becomes an effective elastic system (zero phase lag) with reservoir radius R_{eff} rather than r_0 (Karlstrom et al., 2010), within which viscous stresses are uniform. The spatial viscosity structure that gives rise to this behavior, perhaps a defining feature of magma reservoirs, means that fully viscous crustal response is never realized in our model (red lines in Figure 2D). As shown in supplement section S1, if host rock viscosity is constant, $\mathcal{H}$ does approach the viscous flow limit at large τ. Of course, at long forcing periods and spatial scales much larger that the reservoir we expect that the vertical variation in temperature controls viscous response (e.g., Tromp & Mitrovica, 1999) and our model assumptions are no longer valid. Additional structure in the phase lag spectra may also arise from details of the problem not modeled here (Rucker et al., 2022). But our analytic model captures first-order frequency dependence of the reservoir-crust system effective geometry and bulk rheology on timescales of interest to volcano geodesy.

We also see that crustal thermal structure is imprinted on the transfer function. Chamber depth is approximated by the distance d between surface temperature and chamber boundary T_{in}. Larger T_{in} and d generally result in more pronounced phase lag, with chamber temperature being particularly sensitive (Figure 2A, Figure S3), and noting trade-offs in maximum phase lag between these parameters. Longer forcing periods (lower frequency) require larger effective shells with smaller effective temperatures. Likewise, a hotter crust requires a larger effective shell with larger effective temperature. Although not explored here explicitly, the trajectories in Figure 2D show how variable material coefficients and constitutive model interact: in this case, the background thermal field dictates the range of possible Maxwell viscoelastic response for harmonic forcing functions.

Of course, the discrete shell equivalence explored in Figure 2 is only precise when the pressure forcing is sinusoidal in time. For broadband pressure forcing with more than one frequency as will be explored in the next section, there does not exist a set of values (R_{eff}, T_{eff}) that will allow the effective shell to yield the same response for all frequency components.

4 Signatures of viscoelastic volcano ground deformation

It is useful to demonstrate the utility of the spectral transfer function approach through application to synthetic time-series that mimic geodetic observations. In this section we show examples of maximum vertical surface displacement and crustal strains obtained using the spectral method for various pressurization episodes of a subsurface reservoir.

4.1 Isolated pressurization events

We consider a square pulse forcing time series, pressurizing the chamber for a given duration (episode) above some baseline. This could be considered a simplistic model for a recharge-driven eruption, for example. Elastic surface displacement would be proportional to this chamber pressure (Segall, 2010), however viscous creep causes the displacement be larger and last longer in our model (Figure3a). These differences are directly evident in the displacement frequency spectra (Figure3a). The transfer function increasingly amplifies the spectra at frequencies with periods longer than the characteristic time of the square pulse in this case. Such frequency-dependent amplification results in larger displacement and continuing surface deformation after the end of the episode. Despite the broadband forcing function, viscoelastic response in

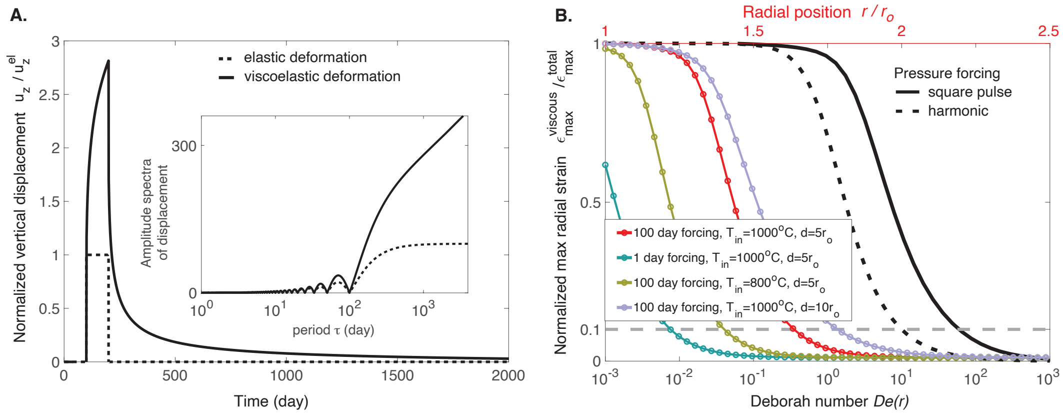

Figure 3. **A.** Maximum vertical ground displacement u_z associated with square pulse pressurization over 100 days with reference viscoelastic parameters (table S1 in Supplementary Material). Dashed lines show the corresponding elastic case. Insert shows amplitude spectra of the normalized displacement obtained from the transfer function as functions of period τ. **B.** Spatial extent of viscous relaxation for square pulse forcing measured by the ratio of maximum deviatoric viscous strain $\epsilon_{max}^{viscous}$ and maximum total deviatoric strain ϵ_{max}^{total}. Horizontal dashed line indicates $\epsilon_{max}^{viscous}/\epsilon_{max}^{total} = 10\%$, an elastic/viscous transition point. The ratio $\epsilon_{max}^{viscous}/\epsilon_{max}^{total}$ is shown as functions of radial position on the top x axis for different parameters (colored lines and markers). These curves collapse (black curves, bottom x-axis) when plotted against spatially variable Deborah number $De(r)$. The elastic/viscous transition corresponds to $De \approx 65$ for square pulse forcing (solid black curve), compared to $De \approx 10$ for harmonic pressurization (dotted black curve).

surface displacement varies with the characteristic time of the pressure forcing: for a rapid pressure forcing event (e.g., a pressurization episode with duration of 1 day), the surface displacement is close to the elastic solution. Conversely for longer pressure forcing (e.g., pressurization episode of one year), the viscoelastic displacement is amplified and the relaxation spectrum exhibits extended temporal lag from input pressure compared with the elastic prediction supplementary Figure S2).

Similar to the harmonic forcing case, the physical origin of this mechanical response can be understood by examining viscous strain around the chamber and the location of effective elastic transition. For linear viscoelastic rheology, the deviatoric strain is the sum of an elastic and a viscous component. We calculate the partition of the total viscous deviatoric strain in space $\epsilon_{max}^{viscous}/\epsilon_{max}^{total}$, which decreases away from the chamber with the background temperature of the crust (Figure 3b colored lines). Viscus relaxation is thus focused around the chamber, with effectively elastic deformation far from the chamber.

We characterize the point where $\epsilon_{max}^{viscous}/\epsilon_{max}^{total} < 10\%$ as an elastic/viscous transition point for the variable coefficient mechanical response to chamber pressurization. With different parameters and different square pulse duration, $\epsilon_{max}^{viscous}/\epsilon_{max}^{total}$ appears to vary spatially (Figure 3B colored curves, top axis). However, the partition between the viscous and elastic components collapses onto a single curve when plotted against local Deborah number (Figure 3B black solid lines, bottom axis). This data collapse indicates 'thermorheologically simple' behavior common in linear viscoelastic systems (Muki & Sternberg, 1961). Rucker et al. (2022) suggest that the extent of significant viscous strain is characterized by a contour associated with $De(r) \approx 10$. This is demonstrated for a single frequency forcing in Figure 3B (black dotted line). However, for broadband square pulse pressure forcing, the corresponding transition boundary is larger, $De \approx 65$ (Figure 3B black solid line).

The dependence of transfer function $\mathcal{H}$ on control parameters suggest possible constraints on thermorheologic and geometrical aspects of the combined magma reservoir-crust system (defining the top of a transcrustal magma transport network, Sparks et al. (2017)) using frequency domain observations. With background temperature as an example, we see in Figure 2 that the 1200°C chamber always amplifies the elastic displacement more strongly than the 800°C chamber. However, the larger relative phase delay between models switches as forcing period increases. The maximum difference in phase delay between 1200°C chamber and 800°C chamber occurs around 3.8 days (Figure S3). For broadband forcing such as the square pulse, such signatures imply specific relationships between deformation frequencies.

4.2 History dependence in event sequences

The frequency dependence of viscoelastic response also implies that sequences of impulsive pressure forcing functions with long period content may exhibit incomplete viscous stress relaxation and thus impart history dependence to the resulting deformation. We demonstrate this time-dependent stress build-up by considering vertical ground deformation response to square pulses of duration t_p in sequence (Figure 4). In the case shown in (Figure 4A), the repose time t_s (e.g., inter-event or hiatus time) between each pressure pulse increases through the sequence. The resulting surface uplift consists of repeated episodes, each with a different peak vertical uplift, despite identical forcing functions. Larger peak displacements occur when the repose time t_s is less than the pressurization pulse duration t_p. But even for the last event in the sequence, occurring after a repose time of twice the pulse duration (100 days), there is amplification relative to an isolated pulse (the amplitude of the first uplift event).

We explore this relationship in more detail in Figure 4B using two square pressure pulses, each with similar t_p but variable t_s. Peak ground deformation relative to an isolated pulse is greater than 1% even for t_s/t_p of 30 (for example, representing $\sim$ 3 month episodes separated by ~ 8 years).

This history dependent behavior is connected again to the extent of viscous relaxation in the crust at the onset of each pressure forcing episode, which involves both the pressurization and repose history. For short repose time, the crust does not have sufficient time to relax before subsequent pressurization occurs, hence the pre-stressed crust results in larger displacement at the end of the second pressurization episode. For large t_s, crustal stress relaxes over a greater range of periods, hence the peak displacement is closer to the previous episode. For the two square pulse case (Figure 4B), the peak surface uplift in the second episode is always higher than the peak uplift during the first episode, which corresponds to a zero-stress, fully-relaxed initial condition. The range of periods for which relaxation can occur is set by the spectrum of Maxwell relaxation times in the crust, determined by the thermal profile in our model. The product of forcing function by the transfer function $\mathcal{H}$ at each period determines its relaxation time.

Incomplete relaxation of forcing signals with significant long-period power is thus likely on timescales of repose times at active volcanoes (e.g., years to centuries). This history dependence implies that the absolute stress state of the crust – a key initial condition for chamber failure or eruption triggering – reflects concurrent magmatism but also magmatic and tectonic history.

5 Summary and Implications

The generality of the Fourier transform and linear superposition make the spectral method presented here attractive for studying time-dependent deformation in magmatic systems. This approach extends commonly used analytic techniques for obtaining viscoelastic solutions from corresponding elastic solutions (e.g., Dragoni & Magnanensi, 1989; Segall, 2016), as Laplace transforms (often used, Fung, 1965) and Fourier transforms agree if the imaginary axis is in the region of absolute convergence of the Laplace transform. As shown in Rucker et al. (2022),

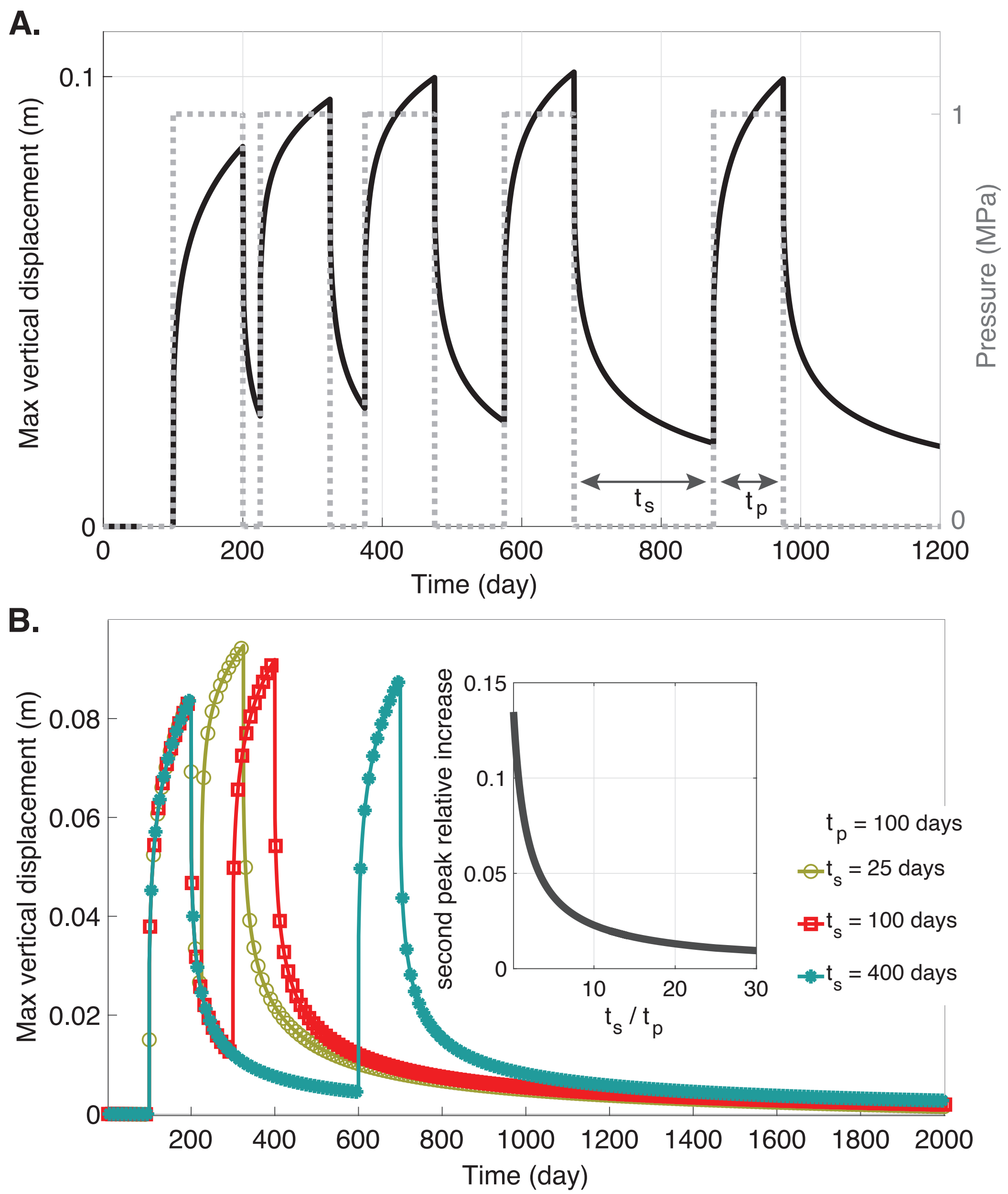

Figure 4. **A.** Maximum vertical ground displacement (solid line, left axis) as a function of time in response to pressure forcing (dash line, right axis) and reference model parameters. Each pressure forcing episode has duration $t_p = 100$ days. The duration of repose time between subsequent pulses are $t_s = 25, 50, 100$, and 200 days. **B.** Ground displacement from two square pressure pulses with variable repose time t_s. Each pulse has a duration of $t_p = 100$ days. Insert shows the relative increase of the peak uplift in the second episode with regard to the peak uplift in the first episode and decreases with repose time.

transfer functions can be obtained numerically, which allows for arbitrary background thermal and material constant heterogeneity, chamber geometry, topography/layering, and tectonic stresses. The advantage of our analytic approach is its physical transparency and efficiency of implementation. Except in unusual cases (Patrick et al., 2019), pressure itself is an unknown quantity (Zhan et al., 2019; Anderson et al., 2020) so reservoir source-time forcing function as well as the transfer function must be inferred from observations. Multiphase magma mass balance and buoyancy impart additional complexity to viscoelastic deformation in general (Segall, 2019; Sigmundsson et al., 2020).

Of course, quantitative details of our results depend on assumed rheology and thermal structure. Here we use a simple radial temperature profile, which approximates expected steady near-surface gradients (supplementary Figure S1) and localized viscoelastic rheology associated with a thermal boundary layer around the chamber. But as numerical explorations show (e.g., Gregg et al., 2013; Head et al., 2021), spatially complex thermal field and specific form of constitutive model exert significant influence on viscoelastic deformation. Although Rucker et al. (2022) demonstrate that the frequency domain structure of transfer function $\mathcal{H}\{u_z|P\}$ found numerically is qualitatively similar to our analytic results, dependence on the spatial distribution of material parameters, domain geometry, and far-field boundary conditions have yet to be established. Additional time-dependent processes, such as poroelasticity (Liao et al., 2018; Mittal & Richards, 2019; Liao, 2022), likely contribute in some cases and could be incorporated into the spectral method developed here.

A more serious problem with this approach is our assumption of steady state geometry and background temperature. The thermal structure of magmatic systems is not steady state on timescales of magmatic evolution (Karakas et al., 2017). This is implied by active lifetimes of mature volcanic centers (100s kyr for stratovolcanoes, Hildreth, 2007), which is smaller than thermal conduction timescale between depths of magma storage and the surface ($d^2/\kappa \sim 800$kyr for $d = 5$km and thermal diffusivity $\kappa = 10^{-6}$ m^2/s) which provides an upper bound on variants in the thermal field. Temperature anomalies that precede eruptions (Girona et al., 2021) suggest far shorter timescales of thermal transience, mediated by fluid advection. Magma reservoir geometry also evolves on a wide range of timescales (e.g., Rivalta et al., 2019; Neal et al., 2019), although large changes in magma storage geometry may be linked to thermorheologic evolution of the crust (Karlstrom et al., 2017; Colón et al., 2018; Huber et al., 2019). Such temporal variations violate the Linear Time Invariant nature of the transfer functions presented here without generalization of the model. For example, evolution of temperature or other scalar fields in the system would require spectral treatment of a more complete set of governing equations.

These caveats aside, we believe that the frequency domain framework outlined here has potential both for observational validation of viscoelastic volcano models, and for enhancing understandings of the diverse deformation patterns seen at volcanoes globally. To argue the first point, we note that the most significant variation in the transfer function occurs in a range of frequencies ($1-100$s days) where geodetic observations are increasingly common. By leveraging the full displacement field (not just maximum vertical displacement presented here) we expect that a variety of transfer functions can be posed and validated with geophysical data. As for the second point, we note that the global distribution of active volcanoes represent diverse snapshots of slowly evolving transcrustal magmatic systems. Identifying quantitative ways in which, for example, a thermally immature versus mature volcanic system should deform as a function of frequency provides concrete predictions that can be used to design experiments and link with exhumed magmatic systems in the geologic record.

6 Open Research

The codes for realizing the results are being uploaded to the public data repository Dryad and will be completed upon resubmission. Codes (matlab) for realizing the results are uploaded as supplementary materials for review purpose.

Acknowledgments

We thank Cody Rucker, Mark Jellinek, Meredith Townsend, and Tushar Mittal for helpful conversations that provided insights to the development of this model. BAE and LK were supported by NSF grant EAR-2036980. LK also acknowledges NSF grant 1848554.

References

Anderson, A. N., Foster, J. H., & Frazer, N. (2020). Implications of deflation-inflation event models on kilauea volcano, hawaii. *Journal of Volcanology and Geothermal Research*, *397*, 106832.

Bakker, R. R., Frehner, M., & Lupi, M. (2016). How temperature-dependent elasticity alters host rock/magmatic reservoir models: A case study on the effects of ice-cap unloading on shallow volcanic systems. *Earth and Planetary Science Letters*, *456*, 16–25. doi: https://doi.org/10.1016/j.epsl.2016.09.039

Biggs, J., & Pritchard, M. E. (2017). Global volcano monitoring: what does it mean when volcanoes deform? *Elements*, *13*(1), 17–22.

Colón, D. P., Bindeman, I. N., & Gerya, T. (2018). Thermomechanical modeling of the formation of a multilevel, crustal-scale magmatic system by the yellowstone plume. *Geophysical Research Letters*, *45*(9), 3873–3879.

Degruyter, W., & Huber, C. (2014). A model for eruption frequency of upper crustal silicic magma chambers. *Earth and Planetary Science Letters*, *403*, 117 - 130. Retrieved from `http://www.sciencedirect.com/science/article/pii/S0012821X14004385` doi: https://doi.org/10.1016/j.epsl.2014.06.047

Del Negro, C., Currenti, G., & Scandura, D. (2009). Temperature-dependent viscoelastic modeling of ground deformation: Application to etna volcano during the 1993–1997 inflation period. *Physics of the Earth and Planetary Interiors*, *172*(3), 299-309. Retrieved from `https://www.sciencedirect.com/science/article/pii/S0031920108003087` doi: https://doi.org/10.1016/j.pepi.2008.10.019

Dragoni, M., & Magnanensi, C. (1989). Displacement and stress produced by a pressurized, spherical magma chamber, surrounded by a viscoelastic shell. *Physics of the Earth and Planetary Interiors*, *56*(3), 316 - 328. Retrieved from `http://www.sciencedirect.com/science/article/pii/0031920189901660` doi: http://dx.doi.org/10.1016/0031-9201(89)90166-0

Fernández, J., Pepe, A., Poland, M. P., & Sigmundsson, F. (2017). Volcano geodesy: Recent developments and future challenges. *Journal of Volcanology and Geothermal Research*, *344*, 1–12.

Fung, Y. C. (1965). *Foundations of solid mechanics* (2nd ed.). Prentice Hall.

Girona, T., Realmuto, V., & Lundgren, P. (2021). Large-scale thermal unrest of volcanoes for years prior to eruption. *Nature Geoscience*, *14*(4), 238–241.

Gregg, P., de Silva, S., & Grosfils, E. (2013). Thermomechanics of shallow magma chamber pressurization: Implications for the assessment of ground deformation data at active volcanoes. *Earth and Planetary Science Letters*, *384*, 100 - 108. Retrieved from `http://www.sciencedirect.com/science/article/pii/S0012821X13005517` doi: https://doi.org/10.1016/j.epsl.2013.09.040

Head, M., Hickey, J., Gottsmann, J., & Fournier, N. (2021). Exploring the impact of thermally controlled crustal viscosity on volcanic ground deformation. *Journal of Geophysical Research: Solid Earth*, *126*(8), e2020JB020724. Retrieved from `https://agupubs.onlinelibrary.wiley.com/doi/abs/10.1029/2020JB020724` (e2020JB020724 2020JB020724) doi: https://doi.org/10.1029/2020JB020724

Hildreth, W. (2007). *Quaternary magmatism in the cascades: Geologic perspectives*. US Geological Survey.

Hou Yip, S. T., Biggs, J., Edmonds, M., Liggins, P., & Shorttle, O. (2022). Contrasting volcanic deformation in arc and ocean island settings due to exsolution of magmatic water. *Geochemistry, Geophysics, Geosystems*, e2022GC010387.

Huber, C., Townsend, M., Degruyter, W., & Bachmann, O. (2019). Optimal depth of subvolcanic magma chamber growth controlled by volatiles and crust rheology. *Nature Geoscience*, *12*(9), 762–768. doi: https://doi.org/10.1038/s41561-019-0415-6

Karakas, O., Degruyter, W., Bachmann, O., & Dufek, J. (2017). Lifetime and size of shallow magma bodies controlled by crustal-scale magmatism. *Nature Geoscience*, *10*(6), 446–450. doi: https://doi.org/10.1038/ngeo2959

Karlstrom, L., Dufek, J., & Manga, M. (2010). Magma chamber stability in arc and continental crust. *Journal of Volcanology and Geothermal Research*, *190*(3), 249-270. Retrieved from `https://www.sciencedirect.com/science/article/pii/S0377027309003977` doi: https://doi.org/10.1016/j.jvolgeores.2009.10.003

Karlstrom, L., Paterson, S. R., & Jellinek, A. M. (2017). A reverse energy cascade for crustal magma transport. *Nature Geoscience*, *10*(8), 604–608. doi: https://doi.org/10.1038/ngeo2982

Kilburn, C. R. (2018). Forecasting volcanic eruptions: Beyond the failure forecast method. *Frontiers in Earth Science*, *6*, 133.

Lambeck, K., Purcell, A., & Zhao, S. (2017). The north american late wisconsin ice sheet and mantle viscosity from glacial rebound analyses. *Quaternary Science Reviews*, *158*, 172–210.

Lau, H. C., & Holtzman, B. K. (2019). "measures of dissipation in viscoelastic media" extended: Toward continuous characterization across very broad geophysical time scales. *Geophysical Research Letters*, *46*(16), 9544–9553.

Lau, H. C. P., Holtzman, B. K., & Havlin, C. (2020). Toward a self-consistent characterization of lithospheric plates using full-spectrum viscoelasticity. *AGU Advances*, *1*(4), e2020AV000205. doi: https://doi.org/10.1029/2020AV000205

Liao, Y. (2022). The roles of heat and gas in a mushy magma chamber. *Journal of Geophysical Research: Solid Earth*, *127*(7), e2022JB024357. Retrieved from `https://agupubs.onlinelibrary.wiley.com/doi/abs/10.1029/2022JB024357` (e2022JB024357 2022JB024357) doi: https://doi.org/10.1029/2022JB024357

Liao, Y., Soule, S. A., & Jones, M. (2018, 2019/03/11). On the mechanical effects of poroelastic crystal mush in classical magma chamber models. *Journal of Geophysical Research: Solid Earth*, *123*(11), 9376–9406. Retrieved from `https://doi.org/10.1029/2018JB015985` doi: 10.1029/2018JB015985

McTigue, D. F. (1987). Elastic stress and deformation near a finite spherical magma body: Resolution of the point source paradox. *Journal of Geophysical Research: Solid Earth*, *92*(B12), 12931–12940. Retrieved from `http://dx.doi.org/10.1029/JB092iB12p12931` doi: 10.1029/JB092iB12p12931

Mittal, T., & Richards, M. A. (2019). Volatile degassing from magma chambers as a control on volcanic eruptions. *Journal of Geophysical Research: Solid Earth*, *124*(8), 7869-7901. Retrieved from `https://agupubs.onlinelibrary.wiley.com/doi/abs/10.1029/2018JB016983` doi: 10.1029/2018JB016983

Mogi, K. (1958, 01). Relations between the eruptions of various volcanoes and the deformations of the ground surfaces around them. *Bull. Earthq. Res. Inst*, *36*.

Muki, R., & Sternberg, E. (1961). On transient thermal stresses in viscoelastic materials with temperature-dependent properties. *J. Appl. Mech.*, *28*.

Neal, C. A., Brantley, S., Antolik, L., Babb, J., Burgess, M., Calles, K., … others (2019). The 2018 rift eruption and summit collapse of kīlauea volcano. *Science*, *363*(6425), 367–374.

O'connell, R., & Budiansky, B. (1978). Measures of dissipation in viscoelastic media. *Geophysical Research Letters*, *5*(1), 5–8. doi: https://doi.org/10.1029/GL005i001p00005

Patrick, M., Swanson, D., & Orr, T. (2019). A review of controls on lava lake level: insights from halema 'uma 'u crater, kīlauea volcano. *Bulletin of Volcanology*, *81*(3), 1–26.

Pollitz, F. F., Peltzer, G., & Bürgmann, R. (2000). Mobility of continental mantle: Evidence from postseismic geodetic observations following the 1992 landers earthquake. *Journal of Geophysical Research: Solid Earth*, *105*(B4), 8035–8054.

Rivalta, E., Corbi, F., Passarelli, L., Acocella, V., Davis, T., & Di Vito, M. A. (2019). Stress inversions to forecast magma pathways and eruptive vent location. *Science advances*, *5*(7), eaau9784.

Rucker, C., Erickson, B. A., Karlstrom, L., Lee, B., & J, G. (2022). A computational framework for time dependent deformation in viscoelastic magmatic systems. *in revision at*

Journal of Geophysical Research Solid Earth. doi: https://doi.org/10.31223/X5WH0N

Schetzen, M. (2003). *Linear time-invariant systems* (1st ed.). The Institute of Electrical and Electronics Engineers.

Segall, P. (2010). *Earthquake and volcano deformation*. Princeton University Press. doi: https://doi.org/10.1515/9781400833856

Segall, P. (2016). Repressurization following eruption from a magma chamber with a viscoelastic aureole. *Journal of Geophysical Research: Solid Earth*, *121*(12), 8501–8522. Retrieved from http://dx.doi.org/10.1002/2016JB013597 (2016JB013597) doi: 10.1002/2016JB013597

Segall, P. (2019). Magma chambers: what we can, and cannot, learn from volcano geodesy. *Philosophical Transactions of the Royal Society A*, *377*(2139). doi: https://doi.org/10.1098/rsta.2018.0158

Sigmundsson, F., Pinel, V., Grapenthin, R., Hooper, A., Halldórsson, S. A., Einarsson, P., ... others (2020). Unexpected large eruptions from buoyant magma bodies within viscoelastic crust. *Nature communications*, *11*(1), 1–11.

Sparks, R. S. J., Cashman, K., & Calais, E. (2017). Dynamic magma systems: Implications for forecasting volcanic activity. *Elements*, *13*(1), 35–40. doi: https://doi.org/10.2113/gselements.13.1.35

Townsend, M. (2022). Linking surface deformation to thermal and mechanical magma chamber processes. *Earth and Planetary Science Letters*, *577*, 117272. Retrieved from https://www.sciencedirect.com/science/article/pii/S0012821X21005288 doi: https://doi.org/10.1016/j.epsl.2021.117272

Tromp, J., & Mitrovica, J. X. (1999). Surface loading of a viscoelastic earth—i. general theory. *Geophysical Journal International*, *137*(3), 847–855.

Zhan, Y., Gregg, P., Le Mével, H., Miller, C., & Cardona, C. (2019). Integrating reservoir dynamics, crustal stress, and geophysical observations of the laguna del maule magmatic system by fem models and data assimilation. *Journal of Geophysical Research: Solid Earth*, *124*(12), 13547–13562.